Biocybernetics and Biomedical Engineering
2010, Volume 30, Number 3, pp. 3–17

Multi-stability of In-phase and Anti-phase Activity Patterns in Neural Networks with Inhibitory and Electrical Synapses

HUBERT OSTASZEWSKI[1], PIERRE MEYRAND[2], PASCAL BRANCHEREAU[2], JOHN HALLAM[3], TIAZA BEM[1,*]

[1]*Nałęcz Institute of Biocybernetics and Biomedical Engineering, Polish Academy of Sciences, Warsaw, Poland*
[2]*Centre de Neuroscience Intégratives et Cognitives, Université Bordeaux 1 and CNRS, France*
[3]*Maersk Mc-Kinney Moller Institute, University of Southern Denmark, Odense, Denmark*

As shown in modeling and experimental studies, network comprised of spiking cells interconnected by inhibitory and electrical synapses may express different activity patterns without any change of the network topology or parameters. In this study we confirm robustness of this phenomenon by demonstrating multi-stability of hybrid networks consisting of biological neurons of different types. Moreover we show here, using relaxation oscillator model cells, that multi-stability of in-phase (IP) and anti-phase (AP) patterns may be expressed in a network fully connected by instantaneous synaptic inhibition and electrical coupling independently of the network size. In such a network a stimulus of a given profile, consisting of depolarizing and hyperpolarizing signals sent to different subpopulations of cells, can evoke direct switching between IP and AP patterns. We also show that similar phenomenon occurs in more realistic network models with sparse connectivity. Our results suggest that transient signals if arriving in a proper time window may instantaneously reconfigure a given spatio-temporal activity pattern expressed by the network into another stable pattern without any change of the network properties.

K e y w o r d s : hybrid network, oscillatory microcircuits, patterns' switching

1. Introduction

Neural networks, as other dynamic systems, can express for a given set of parameters, multiple stable activity patterns and switching between these patterns can be

* Correspondence to: Tiaza Bem, Nałęcz Institute of Biocybernetics and Biomedical Engineering, Polish Academy of Sciences, ul. Ks. Trojdena 4, 02-109 Warsaw, Poland, e-mail: tiaza.bem@ibib.waw.pl
Received 24 September 2009; accepted 4 January 2010

evoked by some external transient input, a phenomenon known as network multi-stability. Although multi-stability has been extensively studied at the level of single cell (for example, plateau activity) providing new understanding of the operation of the neural cell and their consequences on network function [1–5] much less of studies have been devoted to understand multi-stable properties of neural networks. However, modeling studies of dynamics of non-oscillatory networks demonstrated a form of binary memory switch provided by a plateau like activity of the network that can be turn on or off by transient inputs [6–12]. Moreover, in a model of oscillatory network consisting of 2 inhibitory neurons, bi-stability of in-phase (IP) and anti-phase (AP) solutions has been found in the case of slow synaptic kinetics [13] or fast synaptic inhibition combined with electrical coupling [14–17]. Also, conditions of switching between multi-stable patterns as well as properties of switching stimuli have been described in 2, 4 and 6-cell networks fully connected by fast inhibition and electrical coupling [17].

In the present study the robustness of 2-cell network bi-stable properties is confirmed by using different types of biological cells in a hybrid network configuration. Moreover we further investigate multi-stable properties of larger oscillatory networks comprised of relaxation oscillators. We show that in such networks fast inhibition combined with electrical coupling produces multi-stability of IP and AP patterns which co-exist, for a given coupling range, independently of the network size and we demonstrate this phenomenon in a 100-cell network. Moreover, we demonstrate that multi-stability of IP and AP patterns is still expressed in a more realistic network model in which "all to all" type of coupling is replaced by sparse connectivity.

2. Materials and Methods

2.1. Experimental

All biological experiments were performed either on the stomatogastric nervous system of adult lobster *H. gammarus* or neonatal mouse spinal cord.

The lobsters were purchased from fishery supply, and maintained in tanks of aerated recycling seawater kept at 14–15°C. The two commissural ganglia (CoG) were removed from the ventral nerve chain. The isolated CoGs were pinned down in a Sylgard (Dow Corning) lined Petri dish, and continuously superfused with saline held at 12–14°C. The saline composition was (in mM): 479 NaCl, 12.74 KCl, 13.2 $CaCl_2$, 10 $MgSO_4$, 3.9 Na_2SO_4, 5 HEPES (adjusted to pH 7.45 with NaOH). In all experiments, chemical synaptic transmission was blocked using low Ca^{2+} saline (479 NaCl, 12.74 KCl, 3 $CaCl_2$, 10 $MgCl_2$, 3.9 Na_2SO_4, 10 $MnCl_2$, 5 HEPES; adjusted to pH 7.45 with NaOH).

Postnatal P0-P3 OF1 mice (Charles River Laboratories, France) were sacrificed by decapitation, according to protocols approved by the European Community Council and conforming to NIH Guidelines for Care and Use of Laboratory animals.

Postnatal day 0 (P0 = E19.5) corresponded to the date of birth. Brainstem-spinal cord was prepared in the « open-book » configuration as previously described [18]. Briefly, the brainstem-spinal cord was dissected, dorsally opened and meninges were removed. The preparation was placed in the recording chamber and continuously perfused at 30°C ± 2°C (perfusion rate of 3–5 ml/min; chamber volume of 1.5 ml) with an artificial cerebrospinal fluid (ACSF) containing the following (in mM): 113 NaCl, 25 $NaHCO_3$, 11 D-glucose, 4.5 KCl, 2 $CaCl_2$, 1 $MgCl_2$ and 1 NaH_2PO_4 (307 mOsmol/l) (equilibrated with 95%O_2–5%CO_2).

2.2. Electrophysiology

In lobster, intracellular recordings were performed as previously described in [19]. The single Lcell neuron was identified according to its position, size and axonal projections [20]. The membrane potential of the Lcell was monitored with Glass microelectrodes (resistance 20–30 MΩ filled with 2 M potassium acetate), this signal was amplified with Axon Instruments Axoclamp 2B amplifiers (Molecular Devices, Union City, CA) and digitized using a CED device (Cambridge Electronic Design, Cambridge, UK). Data acquisition and analysis were performed using Spike2 Software. Each neuron was impaled with two electrodes, one to monitor the membrane potential, the other for current injection. Artificial synaptic conductances were introduced between the two isolated Lcells using a dynamic clamp system (see [21] for precise procedure). The artificial instantaneous synaptic current i^{syn} ([nA)]) was calculated according to the equation $i^{syn} = g^{syn}\, s(t)(v - v^{syn})$ where g^{syn} ([nS]) is the maximal synaptic conductance, v ([V]) is the cell membrane potential and v^{syn} [V] corresponds to the synaptic reversal potential which was set to –0.05 V. The dynamics of synaptic transmission are described by: $ds(t)/dt = (1 - s(t))/\tau_r - s(t)/\tau_d$, where $s(t)$ is the fraction of transmitter released at time t ([ms]) and τ_r and τ_d ([ms]) are the time constants of the synaptic rise and decay, respectively.

Gap junction current i^{el} ([nA)]) was represented by $i^{el} = g^{el}\,(v - v^p)$ where g^{el} ([nS]) is the gap junction conductance and v^p ([V]) is the membrane potential of the pre-synaptic cell. In order to avoid any tonic compound of the artificial i^{el} an arbitrary offset was added to the recorded voltage so that resting potential of the two cells were equalized to – 0.025 V. Under the dynamic clamp the artificial synaptic current was injected into the (postsynaptic) cell when the membrane potential of the other (presynaptic) cell reaches a given threshold v^{th} (spike detection).

Whole-cell patch-clamp recordings were performed on P0-P3 mouse spinal motoneurons identified according to their morphological features (pear-shaped large cell body) and disposition in column in the ventral horn [18]. An Olympus BX51WI microscope equipped with differential interference contrast (DIC) and a CCD camera (SPOT RT-SE6, Diagnostic Instruments, Sterling Heights, MI, USA) was used to visualize motoneurons. The patch electrodes were constructed from a thin-walled single-filamented borosilicate glass (1.5 mm outer diameter; Harvard Apparatus,

Les Ulis, France) using a two-stage vertical microelectrode puller (PP-830; Narishige, Tokyo, Japan). Pipette resistances ranged from 3 to 5 MΩ and the seal resistances >10 GΩ. Dual whole-cell recordings were achieved using pipettes containing (in mM): 130 Kgluconate, 10 HEPES, 10 EGTA, 5 NaCl, 2 MgATP and 1 $CaCl_2$, pH 7.4 (296 mOsmol/l). The patch electrodes were positioned on visually identified motoneurons using motorized micromanipulators (Luigs & Neumann, Ratingen, Germany). All recordings were made with an AXON Multiclamp 700B amplifier (Molecular Devices, Sunnyvale, CA, USA). Data were low-pass filtered (2.4 kHz) and acquired at 10 kHz on a computer using an analog-to-digital converter (Digidata 1322A; Molecular Devices), and a data acquisition software (Clampex 9.2; Molecular Devices). Measurements were corrected for liquid junction potentials (3.4 mV, calculated using the Clampex Junction Potential Calculator).

2.3. Computational Modeling Methods

2.3.1. The Cell Model

The single cell model is described using a dimensionless relaxation oscillator model, described in details elsewhere [15]. Briefly, the model consists of set of first order differential equations (equation 1–2) in which each cell is represented by two dimensionless state variables: V_i which is the membrane potential deviations of the cell from a reference voltage (this reference value is midway between the depolarized and hyperpolarized voltage ranges during oscillator's intrinsic cycle) and a slow recovery variable W_i dependent on the membrane potential V_i:

$$\tau_v \frac{dV_i}{dt} = -[V_i + W_i - \tanh(G^{fast} V_i) + I_i^{syn} + I_i^{gap} + I_i^{in}(t)] \quad (1)$$

$$\tau_w(V_i) \frac{dW_i}{dt} = -[W_i - G^{slow} V_i]. \quad (2)$$

Dimensionless parameter G^{fast} describes the properties of instantaneous voltage-dependent current (a degree of N-shape, see equation 1) and thereby corresponds to the current's conductance in some range of voltage. Dimensionless parameter G^{slow} models the voltage dependent activation function of the slow current (see equation 2) and is also correlated with the magnitude of the current's conductance. Instantaneous synaptic current I^{syn} (dimensionless) is given by

$$I_i^{syn} = \sum_{j=1}^{j=N} G^{syn} \sigma \left(\frac{V_j - \Theta^{syn}}{k^{syn}} \right) [V_j - E^{syn}] \quad (3)$$

where G^{syn} is the maximal synaptic conductance (scaled by leak conductance) V_j is the membrane potential of the presynaptic cell *j,* E^{syn} is the synaptic reversal potential, Θ^{syn} represents the midpoint for synaptic activation and k^{syn} the steepness

of the synaptic activation function. Function $\sigma(x)$ is given by $\sigma(x) = 1/(1 + e^x)$. Gap junction current is represented by

$$I_i^{syn} = \sum_{j=1}^{j=N} G^{gap}(V_j - V_i) \tag{4}$$

where G^{gap} is electrical conductance (scaled by leak conductance). $I_i^{in}(t)$ is externally injected input current (dimensionless). τ_v and $\tau_w\ (V_i)$ are the membrane time constant and the time constant of slow current dynamics, the latter depending on the membrane potential V_i:

$$\tau_w(V_i) = \tau_2 + (\tau_1 - \tau_2)\sigma\left(\frac{V_i}{k^{tw}}\right) \tag{5}$$

with τ_1 and τ_2 specifying the minimum and maximum time constants and thereby determining the durations of the active and silent phases of the oscillator – and k^{tw} quantifying the rate of voltage dependence.

In the present study following dimensionless parameters are identical for all junctions and neurons: $E^{syn} = -4$, $\Theta^{syn} = 0$, $k^{syn} = 0.02$, $G^{fast} = 2$, $G^{slow} = 2$, $\tau_1 = 5$, $\tau_2 = 50$, $k^{tw} = 0.2$, $\tau_v = 0.16$.

The parameters have been chosen to model neurons with a relatively steep synaptic onset and short duty cycle (i.e. the fraction of the cycle when the cell is depolarised above threshold and may exert synaptic action). With this choice of parameters, equations 1–5 may be considered a model of spiking neurons. In the study presented here, the only parameters varied from the defaults are the dimensionless conductances G^{gap} and G^{syn} of the gap and synaptic junctions, respectively.

The model has been implemented as a set of Matlab functions which compute the quantities defined by the five above-described equations and integrate the set of ordinary differential equations using Matlab's standard ode45 solver with the default tolerance parameter settings. The external input currents $I_i^{in}(t)$ are assumed to be piecewise constant. The implementation has been compared to an independent realisation using a xpp tool and found to give identical results.

2.3.2. Analysis Methods

The investigation of the oscillatory behaviors generated by networks of the type under study is time-consuming and has been automated as much as possible. For a given choice of the conductance parameters, the network dynamics is integrated from a suitable starting state. The first 30% of the simulation following the completion of any non-zero input signal is discarded to mitigate the effects of transients and the membrane potentials are computed at time points with an interval of 0.2 units. Given these values, an attempt is made to estimate a period of regular oscillation for

the network by computing the positions of peaks in the autocorrelation of the signals and looking for recurring inter-peak periods. If this calculation fails, the network is simulated further and the calculation repeated. If no period can be found with simulations up to 3000 units in duration, the signals are reported to be un-analysable. (The typical period of oscillation for the parameters used is 20–25 time units.) Once a period has been determined, the network signals are analysed. Samples for a single period are generated and the traces of the individual cells compared, to group the cells into classes executing the same behavior with possibly differing phases. In all cases reported here, the cells execute the same behavior, that is they all exhibit the same voltage trace to the resolution of the grouping test though their phases within that common trace may vary. Once the cell behaviors have been grouped, the classification of oscillatory modes is performed. The analysis distinguishes the behaviors illustrated in Fig. 2.

For a given choice of the parameters, the network exhibits a number of oscillatory behaviors. In this study, we vary two principal conductance parameters G^{gap} and G^{syn}, over the range in which interesting behaviors occur, for the networks comprising of 2, 4 and 6-cells. The reported results generated as follows for each pair of the parameter values investigated.

(i) a set of 8 random initial states for the network are generated, using a zero mean Gaussian distribution with 0.025 standard deviation. Random current input of length 250 time units is then constructed using independent identically Gaussian distributed random values with zero mean and 0.005 standard deviation for each time step. For each set of the initial conditions the model is integrated with the input current for around 10 periods. Then this input is removed and the behavior of the network that results is analyzed and classified.

(ii) the model is integrated from a zero initial state, and the generation of a IP behavior is checked. If IP is generated, random input current as described above is applied to see whether IP is stable in the presence of noise. The behavior is then classified.

(iv) the model is integrated from a zero initial state as before, and if a stable IP behavior is generated an attempt is made to switch the network to AP: half the cells receive a 1 unit positive current injection and half a 1 unit negative current injection for 0.2 time units, applied at time point between phase $\Phi = 0.4$ and 0.6 in the cycle of oscillation. Again, random current inputs following transient switching impulse are used to verify that the behavior switched to is stable in the presence of noise. The behavior is then classified.

The reported set of behaviors is the union of the results of the three steps above. In our opinion this procedure represents a reasonable compromise between computational effort and completeness of the results. Note, however, that it is not complete: the presence of any particular type of behavior other than AP and IP is only detected if a suitable initial state is chosen (one that lies within the basin of attraction of that behavior) and this cannot be guaranteed.

3. Results

Bi-stability of a 2-cell inhibitory network has been demonstrated in modeling studies either for the slow inhibitory synapses alone [13] or for fast inhibition combined with electrical coupling [14–17]. This later case is illustrated in Fig. 1A, where two model cells (relaxation oscillators) interconnected with both instantaneous inhibition and electrical synapses express IP (Fig. 1A1, IP is indicated by black dots above recordings) or AP (Fig. 1A2) behavior for the same network parameters. Switching between these two patterns can occur spontaneously if noise of sufficient amplitude is introduced to the network (Fig. 1A3). Although this network feature has never been described in a purely biological network, some studies have shown that it can be found in hybrid networks in which biological cells from snail ganglion [16] or cortical slices [22] are interconnected by artificial synapses via a dynamic clamp system. To further explore the robustness of this phenomenon we performed similar experiments using other types of spiking neurons. Our results confirm that bistability of IP and AP behaviors can be easily found in networks comprised of biological neurons. Indeed, as illustrated in Fig. 1B-C, we have found spontaneous switching between AP and IP (see dots) behaviors in networks consisting of 2 lobster Lcells (Fig. 1B) or 2 neonatal mouse motoneurons (Fig. 1C) interconnected by electrical and inhibitory synapses via a dynamic clamp. It must be noted that such behaviors has been observed in all recorded pairs of neurons ($n = 30$ and 6 of Lcells and motoneurons, respectively) by adjusting the strength of inhibitory and electrical conductances.

In the next step, in order to predict the behavior of large-scale networks, we calculated in more details than previously [17] and compared the occurrence of patterns in 2, 4 and 6-cell networks. For 4 and 6-cell networks we used intrinsic cell parameters identical to the 2-cell model network but scaled the synaptic conductance to maintain constant the total synaptic conductance of a single model cell.

In the 6-cell network (Fig. 2A) different types of activity pattern can be found depending on coupling strength (Fig. 2B). Beside IP and AP patterns in which 6 cells' oscillations occur with the phase shift Φ equal 0 (Fig. 2B1) and 0.5 (Fig. 2B2), cells could express phase shift $\Phi < 0.5$ in patterns which we classified depending on the number of expressed phases. For example, in a 2-phase pattern 2 groups of cells express synchronous activity with some phase shift Φ (< 0.5) between the groups containing 1 and 5 cells as in Fig. 2B3 or 2 and 4 cells (not shown). 3-phase pattern is realized by division of the network into 3 groups containing 1, 2 and 3 cells (Fig. 2B4) or 2, 2 and 2 cells (not shown). Similarly 4 and 5-phase pattern contain 4 and 5 groups of cells, respectively (see examples in Fig. 2B5-6) whereas 6-phase pattern consists in each of 6 cells expressing different phase of oscillation (Fig. 6 B7). It should be noted that only in IP and AP patterns cells' trajectories are identical (for example identical voltage traces, or identical two-dimensional trajectories in the phase space (v, W) (see Methods)), we therefore call these patterns symmetrical, whereas other patterns, in which cells trajectories differ, we call asymmetrical. The

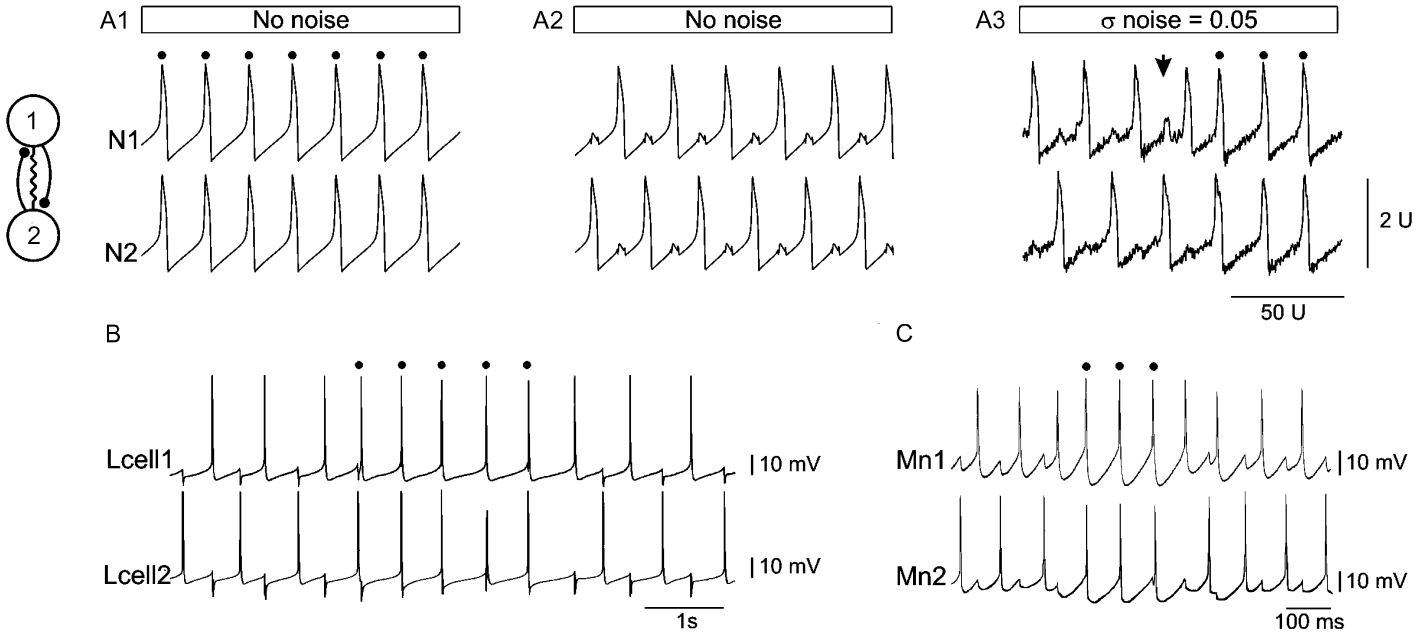

Fig. 1. Bi-stability in the model and hybrid 2-cell networks. The networks consist of two cells interconnected by electrical synapse (resistor symbol in the network diagram) and instantaneous reciprocal inhibitory synapses (solid lines with dots in the network diagram). A: Model network consisting of relaxation oscillators expresses in-phase (IP) (A1), or anti-phase (AP) (A2) activity patterns for the same set of synaptic parameters. Introducing stochastic current input to both cells produces spontaneous transition between the AP and IP (see black dots) patterns (A3). B: Similar spontaneous transition occurs in the patterns expressed by spiking neurons interconnected via dynamic clamp by artificial synapses: Lcells from the commissural ganglion of the lobster nervous system (B) or motoneurons from the pre-natal mouse spinal cord (C). Notice that in (A) time units (U) are arbitrary since the model is dimensionless. Abbreviations: Lcell, Large cell; Mn, motoneuron; N relaxation oscillator model neuron. Parameters: $G^{syn} = 0.032$ (A), $g^{syn} = 2.5$ nS and 5 nS (B), 30 nS (C); $v^{th} = 0$ V (B, C), $\tau_r = 0.5$ ms (B,C), $\tau_d = 7.1$ ms (B), 14 ms (C); $G^{gap} = 0.18$ (A), $g^{el} = 3$ nS (B), the mouse MN were naturally electrically coupled (coefficient of coupling 0.048), σ_noise = 0.05 (A3)

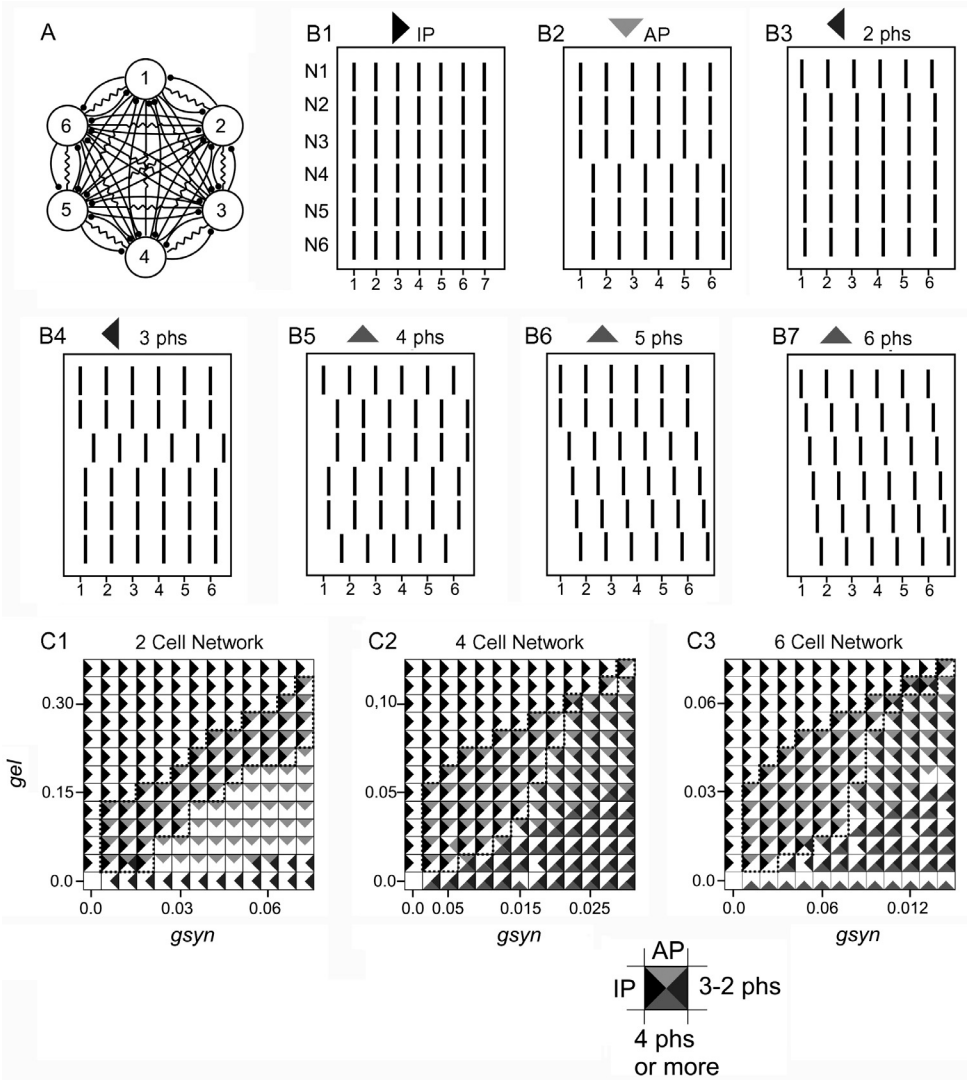

Fig. 2. Multiple stable activity patterns in 2, 4 and 6-cell network. A. Wiring diagram of 6-cell oscillatory network with full synaptic connections. B. Examples of various patterns expressed by the 6-cell network. Timing of oscillations is schematically represented by bars. Two symmetrical patterns: IP (B1) and AP (B2) are characterized by identical trajectory of all network members. Asymmetrical patterns characterized by different cell trajectories can contain from 2 to 6 phases (2 phs, B3 – 6 phs, B7). Notice the synergic group of 2, 3, 4 or 5 cells. C. Occurrence of the activity patterns as a function of synaptic strength in 2 (C1), 4 (C2) and 6 (C3) cell network. Parameters: G^{syn} = 0.014 (B), G^{gap} 0.06 (B1-B2), 0.01 (B3-B4), σ_noise = 0.005, independent identically distributed Gaussian for each 0.2 unit integration step in C

symmetrical IP and AP patterns were expressed in all networks investigated, independently of the network size. By contrast, the number of asymmetrical patterns was reduced with decreasing the network size; only three asymmetrical patterns were

expressed in the 4-cell network (one 4-phase, one 3-phase and one 2-phase pattern) and only one 2-phase pattern was expressed in the 2-cell network (not shown).

The occurrence of the above patterns as a function of the inhibitory and electrical synaptic strength is shown in Fig. 2C. For inhibition alone only the asymmetrical patterns of maximal number of phases are stable: 2-phase pattern in 2-cell network, 4-phase pattern for the 4-cell network and 6-cell pattern for the 6-cell network (see Fig. 2C1-3). Increasing the strength of the electrical coupling G^{gap} produces a reduction of number of phases of the expressed asymmetrical patterns in 4 and 6-cell networks (see a transition from 4 or more phase to 2-3 phase patterns in Fig. 2C2-3) and appearance of the symmetrical AP pattern in all investigated network sizes (Fig. 2C1-3). Further increasing of the electrical coupling leads to appearance of IP behavior until for a sufficiently large G^{gap} AP disappears and only the IP pattern is expressed. Importantly the latter coexists with the AP pattern in similar parameter domains in 2, 4 and 6-cell networks (compare surfaces underlined with dotted lines, Fig. 2C1-3). It seems that such a parameter domain will exist for all networks sizes assuming our scaling the conductance parameters to maintain constant synaptic input to a single cell. This can be explained as follows.

First, the more tightly electrically coupled the cells are the harder is for two groups of cells oscillating in anti-phase to coexist in a stable AP pattern. Indeed, when a cell changes its group memberships due to a noisy input, the symmetry of the pattern is broken. This leads, as a consequence of a fusion of the two groups (asymmetrical patterns are unstable in a region of parameters considered), to IP activity. This determines the 'upper' boundary of the parameter domain, where AP ceases to be expressed. Notice that such a change of memberships is easier in 2 than in 4-cell network, as indicated by a lower position of the 'upper' boundary in the 2-cell network (c.f. Fig. 2C1 and 2C2). How the "upper" boundary will evolve with increasing the network size? Importantly, the change of memberships of a given cell is most likely during firing phases of two groups of cells involved in the AP activity. This is due to the fact that only during these phases the value of the slow recovery current (W, in our cell model, see Methods) is equal for the two groups of cells [15]. Therefore a transition of a cell between groups can be produced quickly, caused only by a change of a membrane potential due to a noisy current. Let's assume now a 2N-cell network expressing alternating activity of the two N-cell groups (AP pattern) and consider the forces acting on a single cell belonging to a given group during a firing phase of the other group. The cell receives inhibition from the N firing cells and, at the same time, is electrically coupled to them. These two factors have opposite effects on a probability of cell's transition between groups: of course, the stronger electrical coupling the most probable the transition. However, the cell is also electrically coupled to N-1 cells of its own group, which prevents it from leaving the group. This coupling conductance is equal to G^{gap} (N – 1)/(2N – 1) and therefore increases from 0 (N = 1) to $G^{gap}/2$ (N infinitive), which increases stability of the AP pattern and moves somewhat up the 'upper' boundary when the network size is raised. The effect is mostly pronounced for the weak inhibition.

A similar reasoning may be applied to a 'lower' boundary of the coexisting IP and AP patterns where IP pattern ceases to be expressed. The IP pattern losses stability when one of cells is able to escape from the synchronous group of cells and to fire in a different phase than the remaining 2N-1 cells. Consider stability of such configuration. When the 2N-1 synchronous cells are firing the single cell is influenced in an opposite way by inhibition (preventing joining the group) and electrical coupling (attracting to the group). Here the total conductance between the single cell and the 2N-1 cells is independent of the network size (and equal for electrical and inhibitory coupling G^{gap} and G^{syn} respectively). However the effect of electrical coupling will decrease with N due to a decreasing of a voltage difference between the membrane potential of the firing group and the cell. Indeed, the voltage amplitude of the cells will be damped by their reciprocal inhibition proportionally to the conductance G^{syn} (2N – 2)/(2N – 1) which increases with increasing network size from 0 (N = 1) to G^{syn} (N infinitive). Thus, the larger N the more stable will be a configuration of a single cell and 2N – 1 synchronous cells and the IP pattern less probable to be expressed. Thus also the 'lower' boundary moves somewhat up as the network size increases. This effect is most visible for strong inhibition. Notice that a biggest shift of a boundary occurs between N = 1 and 2 (c.f. 2 and 4-cell network, Fig. 2C) whereas boundaries for N = 2 and 3 are already very similar (c.f. 4 and 6-cell network, Fig.2C). Therefore both the upper and lower boundaries tend to different limiting position and between them the domain of coexisting IP and AP will always be found, independently of the network size.

This prediction was confirmed in simulation of a large-scale fully connected network in which 100 relaxation oscillators was coupled in "all to all" fashion in such a way that a total synaptic input to a single cell was set within a parameter domain corresponding to the area of coexistence of the IP and AP patterns (Fig. 2C1-3). The matrix of connectivity within the network is illustrated by white areas that illustrates homogenous connections between cells and a black diagonal line which indicates a lack of self-connectivity (Fig. 3A1-2). In such a network, in the presence of stochastic input currents, a synchronous activity can be expressed for arbitrary long time indicating a stability of the pattern (see time 0 to 200 of simulation, Fig. 3A3). Moreover, a transient stimulus (see arrow Fig. 3A3) delivered to network members in a proper moment of the cycle was able to reconfigure the network activity into a stable AP pattern (see time 300 to 600 of simulation, Fig. 3A3).

Importantly moreover, introducing a sparse instead of full connectivity according to the same principle of scaling of total synaptic input to a single cell did not abolish multi-stability of the IP and AP patterns. Indeed, even if the number of synapse existing in a fully connected network is reduced to 50% (or less), the network still expresses the stable IP and AP patterns and a switch between them is produced by a similar transient input (Fig. 3B). However, if number of synapses is reduced to 20% of full connectivity stability of the AP pattern is already lost (Fig. 3C) whereas 5% of synapses did not provide any more neither stable IP nor stable AP behavior (Fig. 3D).

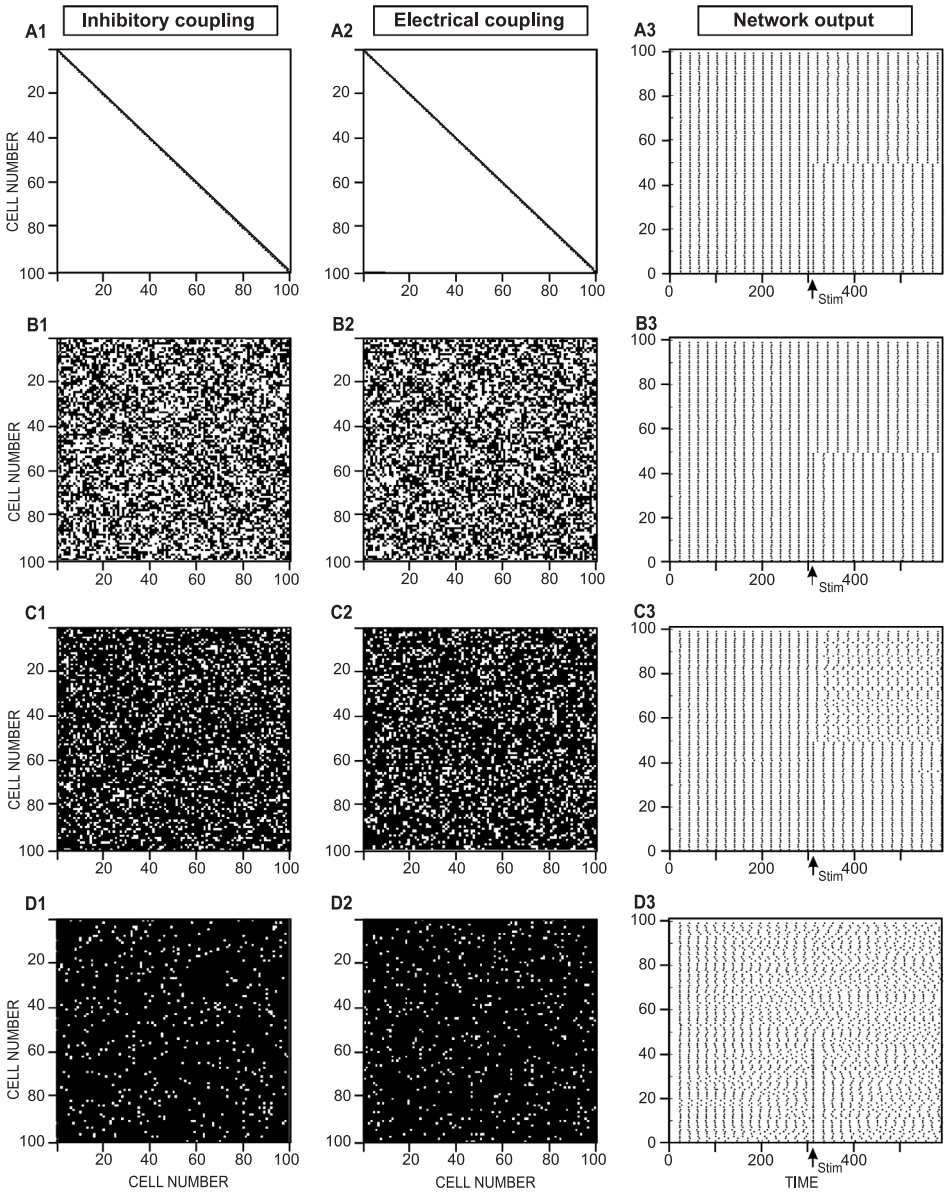

Fig. 3. Multi-stability of the IP and AP patterns in 100-cell network. A. Fully connected network. A1-A2 illustrates distribution of inhibitory and electrical synapses. White areas correspond to existing synapse between cells of given numbers. Black diagonal lines indicate lack of self-connectivity. A3 Raster-diagram of 100 cells shows a transition between the stable IP and AP patterns. This switching is produced by a transient input consisting of excitatory and inhibitory signals delivered to the cells of numbers 1-50 and 51-100, respectively (see black arrow). B-D. Sparsely connected network in which number of connections was reduced to 50% (B), 25% (C) and 5% (D) of full connectivity. The total electrical and inhibitory conductances of a single cell were kept constant. The projections of a single cell to the other network members were distributed randomly (uniform distribution). Whereas in B3 the stimulation identical as in A3 produces the same switching between the IP and AP pattern, it fails to reveal a stable AP in C3. Notice that in D3 the network is unable to express the stable IP or AP pattern. Parameters $G^{gap} = 0.0015$, $G^{syn} = 0.0003$, stimulus intensity = 1, σ_noise = 0.01

4. Discussion

In the present study we demonstrate robustness of multi-stability of the IP and AP activity patterns expressed by neural networks consisting of the biological cells interconnected by inhibitory and electrical synapses. Indeed, this phenomenon was present in L-cells belonging to stomatogastric nervous system of crustaceans as well as in motoneurons of the neonatal mouse spinal cord. These results, together with the previously described occurrence of multi-stable IP and AP patterns in hybrid networks consisting of spiking neurons of snail nervous system [15] and auditory cortex in the mouse [22] indicate that multi-stability can be expressed in neural networks consisting of different types of cells within the central nervous system.

Moreover, we show here that in an oscillatory model network fully interconnected with both fast inhibitory and electrical synapses expression of multi-stabile IP and AP behaviors is independent of the network size and occurs always for some, well defined, range of coupling parameters. Although such a large-scale network generates a large variety of stable activity patterns, number of which depends on the number of cells as well as on the synaptic strength (Fig. 2B) the parameter region where the IP and AP solutions coexist remains the same for all the network sizes if a total synaptic conductance for a single cell is kept constant (see Fig. 2C).

These results become significant in perspective of generalization of switching rules between multi-stable patterns. Indeed, as shown recently, in the parameter sub-space where the IP and AP patterns co-exist the rules for switching between them produced by a transient external signal are similar for 2, 4 and 6-cell networks [17]. Therefore, our results indicate that since a domain of multi-stability of the IP and AP patterns can be always found, the invariance of the switching rules can be extended for all network sizes assuming scaling of the coupling parameters mentioned above.

Robustness of multi-stable behavior of the neural networks is further confirmed by our preliminary results showing multi-stability of the IP and AP behaviors in large scale networks with sparse connectivity (Fig. 3B-C). However, the issue whether rules determining switching between the patterns are the same as in the case of full connections remains to be investigated. Moreover, in the simulations illustrated in Fig. 3 sparseness was introduced in the homogenous way into both inhibitory and electrical connections. As a consequence, a connectivity of a given cell with all the other cells was reduced equally, independently of cell's number and therefore independently of putative space distribution of the cells. However if we consider electrical coupling only between cell bodies as in our model (see Methods) than electrical coupling should take place only between the closest neighbors whereas inhibitory connections could be realized on long distances. On the other hand, some studies underline importance of dendro- and axo-axonal electrical synapses which would provide possibility of long distance electrical coupling between cells [7, 23]. This would require a multi-compartment cell model which was not considered here.

Future study should be undertaken in order to investigate how occurrence of the IP and AP patterns as well as switching between them depend on network topology and type of connectivity, including different localization of electrical synapses within a cell.

5. Conclusions

The present study demonstrates robustness of multi-stability of the basic rhythmic activity patterns that can be generated by inhibitory neural network in the presence of electrical coupling: full synchrony (IP pattern) and anti-synchrony, consisting of alternating activity of two groups of neurons (AP pattern). This indicates that in a large variety of neural networks reconfiguration of network activity may be evoked by transient input, as for example during a transition from one gait to another which can be executed by a transient signal which change instantaneously and simultaneously the phase relationships between all the network elements involved in the task without changing of any of cellular or synaptic properties of the network.

Acknowledgements

This study was supported by MNiSW (status grant 16/st) (TB), by a grant from the Conseil Régional d'Aquitaine (PM, DC) and ANR grant NT051 41718 (PM), by Polonium program (HO, PM, DC, TB), and by Danish Agency for Science, Technology and Innovation (TB and JH grant number 274-06-0292).

References

1. Hultborn H., Brownstone R.B., Toth T.I., Gossard J.P.: Key mechanisms for setting the input-output gain across the motoneuron pool. Prog. Brain Res. 2004, 143, 77–95.
2. Kristan W.B. Jr., Calabrese R.L., Friesen W.O.: Neuronal control of leech behavior. Prog. Neurobiol. 2005, 76, 279–327.
3. Llinas R.R.: The intrinsic electrophysiological properties of mammalian neurons: insights into central nervous system function. Science 1988, 242, 1654–1664.
4. Marder E., Bucher D.: Understanding circuit dynamics using the stomatogastric nervous system of lobsters and crabs. Ann. Rev. Physiol. 2007, 69, 291–316.
5. Meyrand P., Simmers J., Moulins M.: Construction of a pattern-generating circuit with neurons of different networks. Nature 1991, 351, 60–63.
6. Amit D.J., Brunel N.: Model of global spontaneous activity and local structured activity during delay periods in the cerebral cortex. Cereb. Cortex 1997, 7, 237–252.
7. Camperi M., Wang X.J.: A model of visuospatial working memory in prefrontal cortex: recurrent network and cellular bistability. J. Comput. Neurosc. 1998, 5, 383–405.
8. Durstewitz D., Seamans J.K.: Beyond bistability: biophysics and temporal dynamics of working memory. Neuroscience 2006, 139, 119–133.
9. Goldman-Rakic P.S.: Cellular basis of working memory. Neuron 1995, 14, 477–485.

10. Goldman M.S., Levine J.H., Major G., Tank D.W., Seung H.S.: Robust persistent neural activity in a model integrator with multiple hysteretic dendrites per neuron. Cereb Cortex 2003, 13, 1185–1195.
11. Renart A., Song P., Wang X.J.: Robust spatial working memory through homeostatic synaptic scaling in heterogeneous cortical networks. Neuron 2003, 38, 473–485.
12. Zhang K.: Representation of spatial orientation by the intrinsic dynamics of the head-direction cell ensemble: a theory. J Neurosc. 1996, 16, 2112–2126.
13. Van Vreeswijk C., Abbott L.F., Ermentrout G.B.: When inhibition not excitation synchronizes neural firing. J. Comput. Neurosc. 1994, 1, 313–321.
14. Lewis T.J., Rinzel J.: Dynamics of spiking neurons connected by both inhibitory and electrical coupling. J. Comput. Neurosc. 2003, 14, 283–309.
15. Bem T., Rinzel J.: Short duty cycle destabilizes a half-center oscillator, but gap junctions can restabilize the anti-phase pattern. J. Neurophysiol. 2004, 91, 693–703.
16. Bem T., Le Feuvre Y., Rinzel J., Meyrand P.: Electrical coupling induces bistability of rhythms in networks of inhibitory spiking neurons. Eur. J. Neurosc. 2005, 22, 2661–2668.
17. Bem T., Meyrand P., Branchereau P., Hallam J.: Multi-Stability and Pattern-Selection in Oscillatory Networks with Fast Inhibition and Electrical Synapses. PLoS ONE 2008,3(11), e3830. doi:10.1371/journal.pone.0003830
18. Delpy A., Allain A.E., Meyrand P., Branchereau P.: NKCC1 cotransporter inactivation underlies embryonic development of chloride-mediated inhibition in mouse spinal motoneuron. J. Physiol. 2008, 586, 1059–1075.
19. Meyrand P., Simmers J., Moulins M.: Dynamic construction of a neural network from multiple pattern generators in the lobster stomatogastric nervous system. J. Neurosc. 1994, 14, 630–644.
20. Robertson R.M., Moulins M.: A corollary discharge of total foregut motor activity is monitored by a single interneurone in the lobster Homarus gammarus. J. Physiol. (Paris) 1981, 77, 823–827.
21. Sharp A.A., Skinner F.K., Marder E.: Mechanisms of oscillation in dynamic clamp constructed two--cell half-center circuits. J. Neurophysiol. 1996, 76, 867–883.
22. Merriam E.B., Netoff T.I., Banks M.I.: Bistable network behavior of layer I interneurons in auditory cortex. J. Neurosc. 2005, 25, 6175–6186.
23. Traub R.D., Bibbig A.: A model of high-frequency ripples in the hippocampus based on synaptic coupling plus axon-axon gap junctions between pyramidal neurons. J. Neurosc. 2003, 15, 2086–2093.